Additive enabled long-term air stability of tin-based perovskite solar cells

Qidong Tai[†], Xuyun Guo[†], Guanqi Tang[†], Peng You[†], Tsz-wai Ng[‡], Dong Sheng[‡], Jiupeng Cao[†], Chunki Liu[†], Naixiang Wang[†], Ye Zhu[†], Chun-Sing Lee[‡], Feng YAN[†]*

[†]Department of Applied Physics, The Hong Kong Polytechnic University, Hung Hom, Kowloon, Hong Kong, P. R. China

[‡]Center of Super-Diamond and Advanced Films (COSDAF) and Department of Chemistry, City University of Hong Kong, Hong Kong, P. R. China

ABSTRACT: Tin-based perovskites with excellent optoelectronic properties and suitable bandgaps are promising candidates for preparing efficient lead-free perovskite solar cells (PSCs). However, it is challenging to prepare highly stable and efficient tin-based PSCs because Sn^{2+} in perovskites can be easily oxidized to Sn^{4+} upon air exposure. Here we report the fabrication of air stable $FASnI_3$ solar cells by introducing hydroxybenzene sulfonic acid or salt as antioxidant additive into the perovskite precursor solution along with excess $SnCl_2$. The interaction between the sulfonate group and Sn^{2+} ion enables the *in-situ* encapsulation of the perovskite grains with the $SnCl_2$-additive complex layer, which results in greatly enhanced oxidation stability of the perovskite film. The corresponding PSCs are able to maintain 80% of the efficiency over 500 h upon air exposure without encapsulation, which is over ten times longer than the best result reported before. Our results suggest a possible strategy for future design of efficient and stable tin-based PSCs.

■ INTRODUCTION

Perovskite solar cells (PSCs) based on organic-inorganic lead halide perovskites ($APbX_3$, A= Cs^+, methylammonium (MA^+) or formamidinium (FA^+); X = I- or Br^-) have attracted much attention recently for their high efficiency, low cost and facile fabrication processes.[1-4] However, the containing of toxic Pb in the perovskites may prohibit the practical applications of the devices, which triggered studies on lead-free perovskites especially tin-based perovskites ($ASnX_3$).[5-9] The application of tin-based perovskites including $CsSnI_3$,[10-14] $MASnI_3$,[15-19] $FASnI_3$,[20-30] and mixed-organic-cation perovskites[31-38] in PSCs have been reported by several groups. Although the tin-based perovskites show many advantages, such as direct and suitable bandgaps (1.2-1.4 eV), low exciton binding energies and high charge-carrier mobilities, the performance of Sn-based PSCs is inferior to that of Pb-based counterparts due to the oxidative instability of the tin-based perovskites.[9]

Sn^{2+} can be easily oxidized to Sn^{4+} upon air exposure or even in inert atmosphere with trace amount of oxygen, which will result in undesired high conductivity (p-doping) of the perovskite film associated with the formation of Sn vacancies in the perovskite lattice, leading to the failure of Sn-based PSCs.[9, 14, 39] Therefore, it is challenging to achieve Sn-based PSCs with long-term stability. The devices without encapsulation degraded rapidly in ambient air within periods from minutes to hours as reported by different groups. For example, in a study of Zhu et al, the $FASnI_3$ based PSCs degraded completely in 10-20 h in air with relative humidity (RH) of 50%,[23] while in a study of Ito et al, the $FA_{0.75}MA_{0.25}SnI_3$ PSCs failed in 60 min in air. Although many approaches have been adopted in device fabrication, such as the introduction of ethylenediammonium (en) and phenylethylammonium (PEA+) in $FASnI_3$ that can retard O_2 diffusion in perovskites,[22, 34-36] the lifetimes of the PSCs are still far below practical requirements. For instance, PSCs based on PEA^+-doped $FASnI_3$ degraded for over 40% of the initial efficiency after being exposed to ambient air (RH = 20%) for only 76 h.[35] Till now, no effective method can be used to substantially improve the long-term air stability of tin-based PSCs.

Here, we report the greatly enhanced air stability of $FASnI_3$ PSCs by employing hydroxybenzene sulfonic acid or salt thereof as dual-function additives in the presence of excess $SnCl_2$. On one hand, the additives help to eliminate the phase separation induced by $SnCl_2$ due to the formation of $SnCl_2$-additive composites, which encapsulate perovskite grains uniformly. On the other hand, the reducing hydroxybenzene group of the additive molecules would serve as O_2 scavenger (antioxidant) for further protection of the inner perovskite, which is critical to the long-term air stability of the devices. Based on this approach, we obtained very stable $FASnI_3$ PSCs that could retain 80% of their efficiency after being exposed to air for over 500 h without encapsulation, which is more than one order of magnitude longer than the best reported lifetime so far (See supporting information, Table S1). This work offers a facile and effective strategy for fabricating efficient and stable Sn-based PSCs.

■ RESULTS AND DISCUSSION

Figure 1a shows the molecular structures of the three representative additives used in our work, including phenolsulfonic acid (PSA), 2-aminophenol-4-sulfonic acid (APSA), and the potassium salt of hydroquinone sulfonic acid (KHQSA). Here,

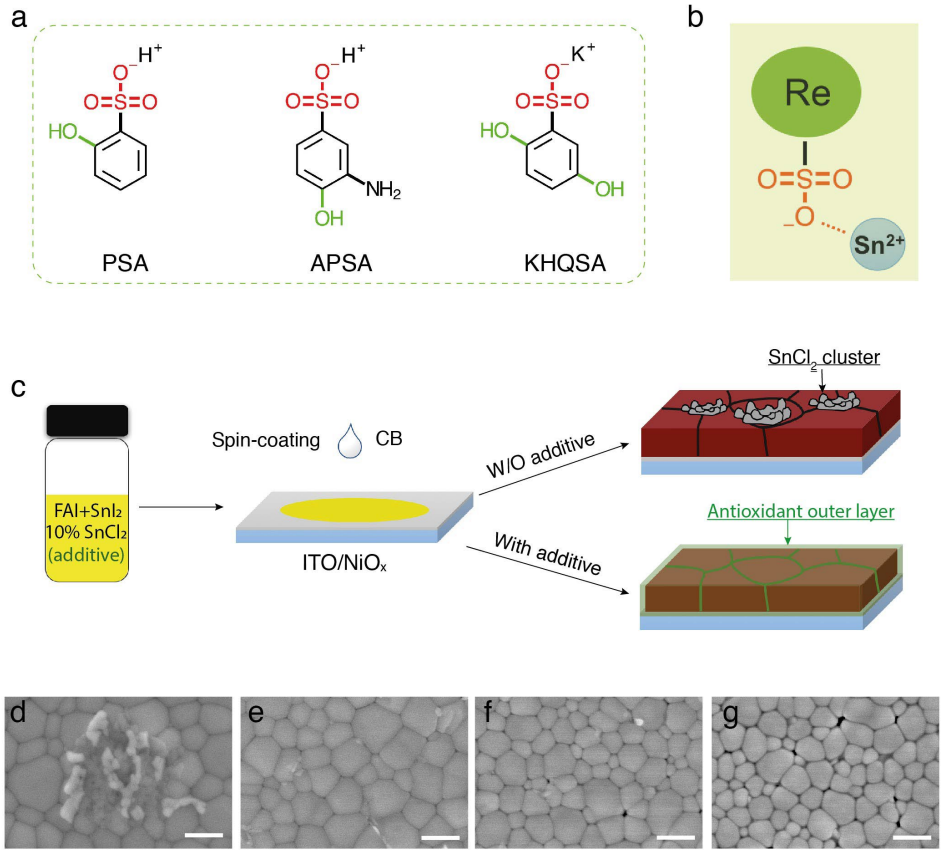

Figure 1. (a) molecular structures of PSA, APSA and KHQSA. (b) schematic illustration of the interaction between the additive molecule and Sn^{2+} ion. (c) Schematic illustration of the method for perovskite film preparation and the morphologies of the perovskite films with and without additive. (d-g) SEM images of the pristine, 1.5%, 3% APSA, and 5% KHQSA-modified $FASnI_3$ films and the scale bar is 500 nm.

PSA could be regarded as a benchmark material, in which the reducing hydroxybenzene group endows it with antioxidant activity that is useful for preventing the Sn^{2+} oxidation[40] and the sulfonate group (SO_3^-) could interact with Sn^{2+} in solution via coordination interaction and electrostatic attraction,[41-42] as illustrated in Figure 1b. In comparison, APSA with an extra Lewis basic amino ($-NH_2$) group should have stronger interaction with Sn^{2+};[43] while the KHQSA that contains two hydroxyl (-OH) groups would have higher antioxidant activity.[44-45]

Figure 1c shows the procedure for preparing $FASnI_3$ films with an additive and 10% excess $SnCl_2$. In the pristine perovskite film without the additive, $SnCl_2$ tends to form large aggregates (~1 μm) (Figure 1d and Figure S1), which is detrimental to the performance of PSCs. In contrast, the formation of $SnCl_2$ aggregates was considerably reduced by introducing only a small amount (1.5 mol %) of the additive into the precursor solution (Figure 1e and Figure S2a, 2d), which can be attributed to the formation of $SnCl_2$-additive complex owing to the interaction between SO_3^- group and Sn^{2+}.

To clarify the interaction between $SnCl_2$ and SO_3^- group of the additive molecules, pure $SnCl_2$ and $SnCl_2$-KHQSA composite films were prepared. As displayed in Figure S 3a, b, the $SnCl_2$ film was rather rough for the easy formation of large branched crystals, while a smooth and homogeneous morphology was observed for the KHQSA-$SnCl_2$ composite film in which the crystallization of $SnCl_2$ was greatly suppressed (Figure S 3c). A further study of the composite film through FTIR provided the direct evidence for the interaction of SO_3^- and $SnCl_2$, since the bands related to the stretching vibration of SO_3^- at 1174 (ν_{as}), 1080 (ν_s), and 1020 cm^{-1} (ν_s) for KHQSA were shifted to higher wavenumbers at 1203, 1110, and 1066 cm^{-1}, respectively. Besides, the new band appeared at 991cm^{-1} was assigned to stretching of S-O (Figure S 3d). The observed changes of the FTIR bands stemmed from the decreased spatial symmetry of SO_3^- due to the coordination of Sn^{2+}.[42, 46]

Figure 1e-g present the SEM images of perovskite films containing different amount of KHQSA. It is found that the perovskite grain size decreases slightly with the increased addition of KHQSA, while the distance between individual grains becomes larger, suggesting the existence of the KHQSA molecules at the grain boundaries and surfaces. Similar phenomenon was also observed in the case of PSA and APSA additions (Figure S2). Notably, a pronounced decrease of grain size was found in the APSA modified perovskite films, which can be explained by the suppression of the fast nucleation due to the stronger interaction between APSA molecule and Sn^{2+} than in the other two cases.[42]

Figure 2a and 2b show the absorption spectra and XRD patterns of $FASnI_3$ films with different additives, respectively. Notably, the additives do not lead to detectable changes in the curves, which suggests that the additive molecules are not incorporated into the perovskite lattice. In order to identify the spatial distribution of the additives in the perovskite film, we

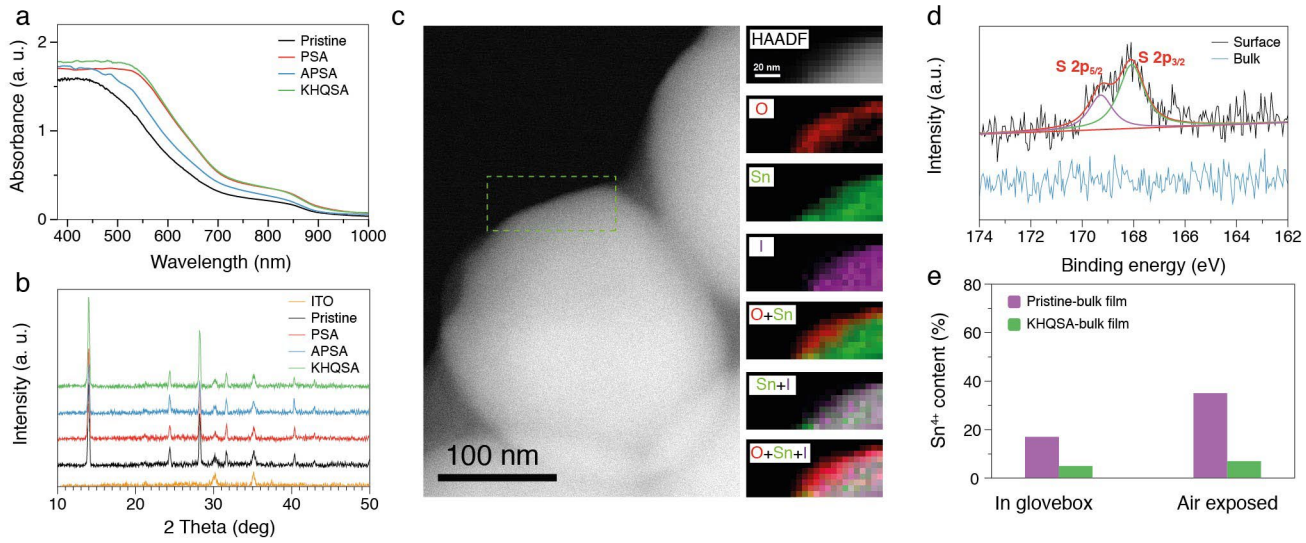

Figure 2. (a) Absorbance and (b) XRD patterns of the pristine, 3% PSA, 3% APSA, and 1.5% KHQSA-modified $FASnI_3$ films. (c) STEM-HAADF images and the STEM-EELS maps of the O, Sn, I, corresponding the 10% KHQSA modified $FASnI_3$ film (no $SnCl_2$). (c) XPS S 2p spectra measured from the surface and the bulk of 1.5% KHQSA-modified $FASnI_3$ film. (d) Sn^{4+} contents determined from bulk of the pristine and 1.5% KHQSA-modified $FASnI_3$ films after they were exposed to dry air (RH = ~20%) for 10 h, similar films stored in glovebox were characterized as reference.

performed scanning transmission electron microscopy (STEM) characterization together with electron energy loss spectra (EELS) by taking KHQSA as an example. In our experiment, O K-edge was used to identify the KHQSA molecules in $FASnI_3$ perovskite. In a parallel study, pure $FASnI_3$ film was also characterized but no obvious O K-edge signal was found (Figure S4). Figure 2c shows STEM image and the corresponding EELS maps of O and the characteristic Sn, I elements of the $FASnI_3$ perovskite. From the superposition of these three characteristic elements, a distribution of the KHQSA on the perovskite grain surface can be clearly observed.

The surface concentrated behavior of the additive molecules was further confirmed via X-ray photoelectron spectroscopy (XPS) characterization. As shown in Figure 2d, the S 2p signal that can be detected from the surface of the perovskite film disappeared after the film was etched with argon ion. Similar depth dependence of the XPS signal was also observed for Cl 2p (Figure S5), indicating again that Cl was not incorporated into the $FASnI_3$ lattice, which was consistent with our previous observation. Based on all the evidences we have observed so far, it is reasonable to conclude that the additive strategy would lead to the in-situ encapsulation of the $FASnI_3$ grain by $SnCl_2$-additive complex layer, which could be highly advantageous for the stability of the inner perovskite. As a demonstration, we compared the Sn^{4+} contents in the pristine and 1.5% KHQSA modified FASnI3 films after they were exposed to air (RH = ~20%). Meanwhile, similar films stored in the glovebox were also characterized as reference. The contents of Sn^{4+} were determined by deconvolution of the XPS spectra of Sn 3d, and the presented data (Figure S6) were recorded after the perovskite films were etched with 2 KeV argon ion for 60s to exclude the influence of unintentional surface oxidation.[21, 34] As shown in Figure 2e, the Sn^{4+} content was considerably lower in the KHQSA-$FASnI_3$ film, indicating a greatly suppressed Sn^{2+} oxidation, which could be due to the retarded O_2 diffusion in the perovskite film.

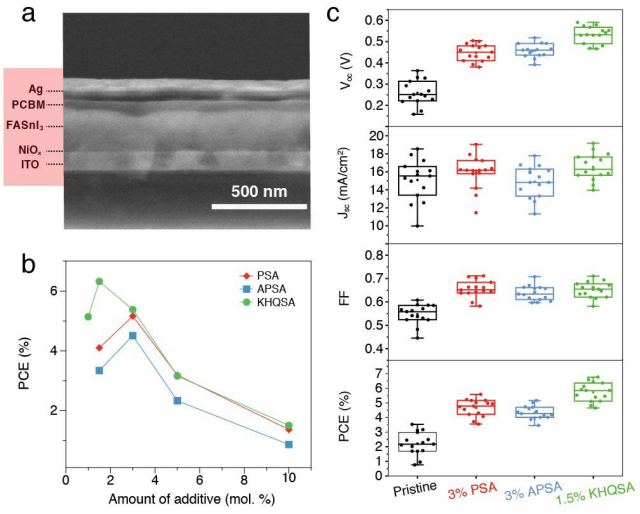

Figure 3. (a) Cross-sectional SEM image of a completed PSC as an illustration of the device structure used in our work. (b) PCE-dose dependence of $FASnI_3$ based PSCs with different amounts of PSA, APSA, and KHQSA additives. (c) statistical photovoltaic performance of $FASnI_3$ based PSCs modified with optimal amount of PSA, APSA, and KHQSA.

PSCs with an inverted device structure of ITO/NiO_x/$FASnI_3$/PCBM/Ag (Figure 3a) were fabricated to study the photovoltaic performance of $FASnI_3$ films with different additives. As presented in Figure 3b and Figure S7, similar dose-dependence of PCE is observed for PSA, APSA, and KHQSA, which can be attributed to the following reasons. First, a certain amount of additive (>1 mol %) is required to prevent the phase separation of $SnCl_2$ and the oxidation of the perovskite; However, too much additive ($\geqslant$5 mol%) can dramatically decrease the photocurrent because the complex located at perovskite grain boundaries and surfaces is less con-

ductive. Hence, suitable amount of additives can lead to the maximum PCE. Both PSA and APSA were found to be optimal at 3 mol %, while the KHQSA was optimal at smaller amount of 1.5 mol%. It is reasonable since KHQSA has higher antioxidant activity and thus is able to offer sufficient protection of the perovskite at a lower concentration. Due to the difficulty in obtaining high-quality $FASnI_3$ films, the pristine devices without any additives only showed an average PCE of 2.2 ± 0.76% with its maximum value of 3.53%. Upon additive strategy, the average PCEs were significantly improved to 4.67 ± 0.57%, 4.33 ± 0.44%, and 5.73 ± 0.63% together with the champion values of 5.58 %, 5.16%, and 6.76%, in the case of PSA, APSA, and KHQSA, respectively (Figure 3d and Table 1). The improved PCE is mainly ascribed to the enhanced open-circuit voltage (V_{oc}) and fill factor (*FF*). The champion PCE obtained from the KHQSA-PSC is comparable to the best results reported for the $FASnI_3$-based PSCs.[23-25]

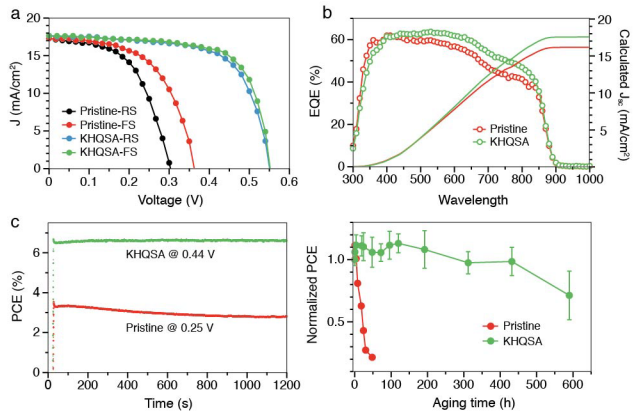

Figure 4. (a) *J-V* curves, (b) EQE spectra, and (c) stabilized power outputs of the best-performing pristine and KHQSA-modified $FASnI_3$ solar cells. (d) stability of the pristine and KHQSA-modified solar cells upon exposure in dry air (RH = ~20%) in dark without device encapsulation.

Figure 4a shows the J-V curves of the best-performing pristine and KHQSA modified PSCs. The corresponding external quantum efficiency (EQE) spectra are presented in Figure 4b. The J_{sc} calculated from the EQE spectrum of KHQSA-PSC is 17.53 mA/cm^2, which is close to measured value of 17.64 mA/cm^2. While the calculated J_{sc} (16.17 mA/cm^2) of the pristine PSC is much lower than the measured J_{sc} (17.3 mA/cm^2), probably due to the degradation of the device in ambient air during the measurement. Compared with the large *J-V* hysteresis shown in the pristine PSC, little hysteresis was observed for the KHQSA-PSC due to the lower trap density of the perovskite film as revealed by PL measurement (Figure S8). In addition, the KHQSA-PSC showed a stabilized PCE of 6.6% within 1200s maximum power point tracking, while the pristine PSC degraded gradually from the initial PCE of 3.3 to 2.8% (Figure 4c), indicating better stability of the former.

Figure 4d compares the stability of the pristine and KHQSA-PSCs corresponding to the exposure of the unencapsulated devices to air (RH = ~ 20%) in dark. Due to the easy oxidation of Sn^{2+}, the pristine devices degraded rapidly in 48 h, with an 80% loss of the average PCE. In striking contrast, the average PCE of the KHQSA-PSCs maintained over 80% for more than 500 h, in consistent with our previous observation of the significantly suppressed Sn^{2+} oxidation in the KHQSA-$FASnI_3$ film. Similarly, prolonged air stability was also observed for the PSA and APSA -modified devices (Figure S9). In comparison with the reported lifetimes of Sn – based PSCs in air,[xxx] our devices show a lifetime over ten times longer (See supporting information, Table S1).

We also performed light soaking (100 mW/cm^2) tests of the pristine and KHQSA-PSCs in air without encapsulation. As displayed in Supporting information (Figure S10), the pristine PSCs showed a fast 50% efficiency-loss in 1.5 h, while the KHQSA-PSCs took 10 times longer time to lose the same percentage of the initial efficiency. In addition, severe corrosion of the Ag electrodes was found in the pristine PSC as shown by the photo of the device taken at 3.5 h (see the inset in Figure S10), which can be ascribed to the reaction of iodine containing volatile species (FAI and/or HI) with Ag, caused by the decomposition of the perovskite. Actually, this is a common problem for the application of Ag electrodes in perovskite containing devices.[47] On the other hand, the Ag electrodes in the KHQSA-PSCs were intact after being exposed to light for the same period of time, due to the surface passivation of the perovskite. This result suggests that our method can also be applied to improve the long-term operation stability of conventional Pb-based PSCs when Ag electrodes are used.

It is notable that the antioxidant property of the additive is critical to the device performance. We can find that KHQSA with more hydroxyl groups on the benzene ring (higher antioxidant activity) leads to the highest device efficiency and the longest device stability, in comparison with the effects of PSA and APSA. To further highlight this point, we designed a control experiment, in which benzene sulfonic acid (BSA) that of no hydroxyl group on the benzene ring was used as an additive. As shown in Figure S11, BSA was also able to suppress the $SnCl_2$ phase separation. However, the corresponding PSCs only showed a champion PCE of 4.11%, lower than that obtained with PSA, APSA, and KHQSA. Furthermore, the BSA containing PSCs degraded much faster in air, which lost over 60% of the initial PCE after being exposed in air for only 48 h. This result suggests the existence of the reducing hydroxybenzene group is very important to both device efficiency and stability.

■ CONCLUSION

In summary, we demonstrate a strategy for fabricating stable $FASnI_3$ based PSCs by introducing several antioxidant hydroxybenzene sulfonic acids or salts as additives into $SnCl_2$ containing perovskite precursor solutions, which results in the in-situ encapsulation of the perovskite grains with $SnCl_2$-additive complex layer, rendering a significantly improved oxidation stability of the perovskite film and the corresponding PSCs. The lifetime of the resultant Sn-based PSCs in air is more than ten times longer than those reported in literature. It is expected that such convenient strategy can be effectively used in other Sn-based perovskites to improve the device stability and efficiency.

■ EXPERIMENTAL SECTION

Preparation of NiO_x film. NiO_x nanoparticles (NPs) were synthesized by following a procedure reported elsewhere,[47] the as-prepared NiO_x NPs were then dispersed in D. I. water at a concentration of 7.5 mg/ml. After being filtered with 0.45 μm

nylon filter, the colloid solution was spin-coated on the ITO substrate at 4000 rpm for 30 s. Then the NiO_x film was annealed on a hotplate at 150 ℃ for 30 min in air.

Fabrication of $FASnI_3$ solar cells. A precursor solution composed of 1 M SnI_2 (Youxuan tech. 99.99%), 1 M FAI, 1 M DMSO, 0.1 M $SnCl_2$ (Aladdin, 99%), and a certain amount of HBSA (Sigma-Aldrich) in DMF was first prepared. Then the precursor solution was spin-coated on the NiOx/ITO substrate at 5000 rpm for 30 s, during which chlorobenzene (CB) was quickly dripped onto the substrate at 11s from the start. The perovskite film was then annealed at 70 ℃ for 5 min, followed by the spin-coating of the $PC_{71}BM$ layer from a 20 mg/ml CB solution at 1500 rpm for 60 s. Finally, a 100-nm-thick Ag electrode was evaporated. All of the procedures were conducted in a N_2-filled glovebox.

Characterizations. The absorbance, XRD, and SEM characterizations of the perovskite film were conducted on Hitachi UH5300 spectrophotometer, Rigaku SmartLab X-Ray diffractometer, and JEOL JSM 6335F SEM, respectively. FTIR spectra were measured by using Bruker VERTEX 70 FT-IR spectrometer. The XPS spectra were obtained by VG ESCLAB 220i- XL surface analysis system equipped with a monochromatic Al K α X-ray source (1486.6 eV). Steady-state and time resolved photoluminescence (PL) spectra were measured on Edinburgh FLSP920 fluorescence spectrophotometer with an excitation wavelength of 635 nm. STEM characterization was performed using JEOL JEM-2100F TEM/STEM operated at 200 kV, using Gatan Enfina electron spectrometer (CA, USA). EELS spectrum imaging was conducted under 200 kV accelerating voltage with an optimal 13 mrad convergence angle. The TEM samples were prepared by a direct deposition of the perovskite film on the carbon-coated TEM grid using the same method as we used on NiO_x/ITO substrate. The J–V curves of the PSCs were recorded under 100 mW/cm^2 AM 1.5G simulated illumination (Oriel 91160). The EQE spectra were obtained using an EQE system equipped with a xenon lamp (Oriel 66902), a monochromator (Newport 66902), a Si detector (Oriel 76175_71580), and a dual-channel power meter (Newport 2931_C). The J-V and EQE characterizations were performed in ambient air without encapsulation of the devices.

ASSOCIATED CONTENT

Supporting Information

The Supporting Information is available free of charge on the ACS Publications website.

SEM images of the pristine and PSA, APSA-modified $FASnI_3$ films; optical microscopy, XRD and FTIR characterizations of $SnCl_2$ and $SnCl_2$-KHQSA composite films; EELS, XPS, and PL characterizations of pristine and KHQSA-moidified $FASnI_3$ films; J-V curves of the PSA, APSA, and KHQSA-PSCs; long-term air stability of PSA and APSA-PSCs; light-soaking stability of pristine and KHQSA-PSCs; SEM image of BSA modified $FASnI_3$ film, J-V cure of the corresponding champion device, and the long-term device stability in air; tables (PDF)

AUTHOR INFORMATION

Corresponding Author

* apafyan@polyu.edu.hk

Notes

The authors declare no competing financial interest.

ACKNOWLEDGMENT

This work is financially supported by the Research Grants Council (RGC) of Hong Kong, China (Project No. PolyU 152087/17E) and the Hong Kong Polytechnic University (Project No. 1-ZVGH).

REFERENCES

(1). Jeon, N. J.; Na, H.; Jung, E. H.; Yang, T.-Y.; Lee, Y. G.; Kim, G.; Shin, H.-W.; Il Seok, S.; Lee, J.; Seo, J., Nature Energy 2018, 3, 682-689.
(2). Yang, W. S.; Park, B.-W.; Jung, E. H.; Jeon, N. J.; Kim, Y. C.; Lee, D. U.; Shin, S. S.; Seo, J.; Kim, E. K.; Noh, J. H.; Seok, S. I., Science 2017, 356, 1376.
(3). Grätzel, M., Acc. Chem. Res. 2017, 50, 487-491.
(4). Correa-Baena, J.-P.; Saliba, M.; Buonassisi, T.; Grätzel, M.; Abate, A.; Tress, W.; Hagfeldt, A., Science 2017, 358, 739.
(5). Giustino, F.; Snaith, H. J., ACS Energy Lett. 2016, 1, 1233-1240.
(6). Abate, A., Joule 2017, 1, 659-664.
(7). Liang, L.; Gao, P., Adv. Sci. 2017, 5, 1700331.
(8). Shi, Z.; Guo, J.; Chen, Y.; Li, Q.; Pan, Y.; Zhang, H.; Xia, Y.; Huang, W., Adv, Mater. 2017, 29, 1605005.
(9). Konstantakou, M.; Stergiopoulos, T., J. Mater. Chem. A 2017, 5, 11518-11549.
(10). Marshall, K. P.; Walker, M.; Walton, R. I.; Hatton, R. A., Nature Energy 2016, 1, 16178.
(11). Wang, N.; Zhou, Y.; Ju, M.-G.; Garces, H. F.; Ding, T.; Pang, S.; Zeng, X. C.; Padture, N. P.; Sun, X. W., Adv, Energy Mater. 2016, 6, 1601130.
(12). Song, T.-B.; Yokoyama, T.; Stoumpos, C. C.; Logsdon, J.; Cao, D. H.; Wasielewski, M. R.; Aramaki, S.; Kanatzidis, M. G., J. Am. Chem. Soc. 2017, 139, 836-842.
(13). Song, T.-B.; Yokoyama, T.; Aramaki, S.; Kanatzidis, M. G., ACS Energy Lett. 2017, 2, 897-903.
(14). Kumar, M. H.; Dharani, S.; Leong, W. L.; Boix, P. P.; Prabhakar, R. R.; Baikie, T.; Shi, C.; Ding, H.; Ramesh, R.; Asta, M.; Graetzel, M.; Mhaisalkar, S. G.; Mathews, N., Adv, Mater. 2014, 26, 7122-7127.
(15). Hao, F.; Stoumpos, C. C.; Cao, D. H.; Chang, R. P. H.; Kanatzidis, M. G., Nature Photonics 2014, 8, 489.
(16). Noel, N. K.; Stranks, S. D.; Abate, A.; Wehrenfennig, C.; Guarnera, S.; Haghighirad, A.-A.; Sadhanala, A.; Eperon, G. E.; Pathak, S. K.; Johnston, M. B.; Petrozza, A.; Herz, L. M.; Snaith, H. J., Energy Environ. Sci. 2014, 7, 3061-3068.
(17). Yokoyama, T.; Cao, D. H.; Stoumpos, C. C.; Song, T.-B.; Sato, Y.; Aramaki, S.; Kanatzidis, M. G., J. Phys. Chem. Lett. 2016, 7, 776-782.
(18). Ke, W.; Stoumpos, C. C.; Spanopoulos, I.; Mao, L.; Chen, M.; Wasielewski, M. R.; Kanatzidis, M. G., J. Am. Chem. Soc. 2017, 139, 14800-14806.
(19). Yokoyama, T.; Song, T.-B.; Cao, D. H.; Stoumpos, C. C.; Aramaki, S.; Kanatzidis, M. G., ACS Energy Lett. 2017, 2, 22-28.
(20). Liao, W.; Zhao, D.; Yu, Y.; Grice, C. R.; Wang, C.; Cimaroli, A. J.; Schulz, P.; Meng, W.; Zhu, K.; Xiong, R.-G.; Yan, Y., Adv, Mater. 2016, 28, 9333-9340.
(21). Lee, S. J.; Shin, S. S.; Kim, Y. C.; Kim, D.; Ahn, T. K.; Noh, J. H.; Seo, J.; Seok, S. I., J. Am. Chem. Soc. 2016, 138, 3974-3977.
(22). Ke, W.; Stoumpos, C. C.; Zhu, M.; Mao, L.; Spanopoulos, I.; Liu, J.; Kontsevoi, O. Y.; Chen, M.; Sarma, D.; Zhang, Y.; Wasielewski, M. R.; Kanatzidis, M. G., Sci. Adv. 2017, 3, e1701293.
(23). Zhu, Z.; Chueh, C.-C.; Li, N.; Mao, C.; Jen, A. K. Y., Adv, Mater. 2017, 30, 1703800.

(24). Chen, K.; Wu, P.; Yang, W.; Su, R.; Luo, D.; Yang, X.; Tu, Y.; Zhu, R.; Gong, Q., Nano Energy 2018, 49, 411-418.
(25). Gu, F.; Ye, S.; Zhao, Z.; Rao, H.; Liu, Z.; Bian, Z.; Huang, C., Solar RRL 2018, 0, 1800136.
(26). Liu, X.; Wang, Y.; Xie, F.; Yang, X.; Han, L., ACS Energy Lett. 2018, 3, 1116-1121.
(27). Lee, S. J.; Shin, S. S.; Im, J.; Ahn, T. K.; Noh, J. H.; Jeon, N. J.; Seok, S. I.; Seo, J., ACS Energy Lett. 2018, 3, 46-53.
(28). Kayesh, M. E.; Chowdhury, T. H.; Matsuishi, K.; Kaneko, R.; Kazaoui, S.; Lee, J.-J.; Noda, T.; Islam, A., ACS Energy Lett. 2018, 3, 1584-1589.
(29). Ke, W.; Priyanka, P.; Vegiraju, S.; Stoumpos, C. C.; Spanopoulos, I.; Soe, C. M. M.; Marks, T. J.; Chen, M.-C.; Kanatzidis, M. G., J. Am. Chem. Soc. 2018, 140, 388-393.
(30). Ke, W.; Stoumpos, C. C.; Spanopoulos, I.; Chen, M.; Wasielewski, M. R.; Kanatzidis, M. G., ACS Energy Lett. 2018, 3, 1470-1476.
(31). Zhao, Z.; Gu, F.; Li, Y.; Sun, W.; Ye, S.; Rao, H.; Liu, Z.; Bian, Z.; Huang, C., Adv. Sci. 2017, 4, 1700204.
(32). Ito, N.; Kamarudin, M. A.; Hirotani, D.; Zhang, Y.; Shen, Q.; Ogomi, Y.; Iikubo, S.; Minemoto, T.; Yoshino, K.; Hayase, S., J. Phys. Chem. Lett. 2018, 9, 1682-1688.
(33). Liu, J.; Ozaki, M.; Yakumaru, S.; Handa, T.; Nishikubo, R.; Kanemitsu, Y.; Saeki, A.; Murata, Y.; Murdey, R.; Wakamiya, A., Angew. Chem. Int. Ed. 2018, 57, 13221-13225.
(34). Liao, Y.; Liu, H.; Zhou, W.; Yang, D.; Shang, Y.; Shi, Z.; Li, B.; Jiang, X.; Zhang, L.; Quan, L. N.; Quintero-Bermudez, R.; Sutherland, B. R.; Mi, Q.; Sargent, E. H.; Ning, Z., J. Am. Chem. Soc. 2017, 139, 6693-6699.
(35). Shao, S.; Liu, J.; Portale, G.; Fang, H.-H.; Blake, G. R.; ten Brink, G. H.; Koster, L. J. A.; Loi, M. A., Adv, Energy Mater. 2017, 8, 1702019.
(36). Jokar, E.; Chien, C.-H.; Fathi, A.; Rameez, M.; Chang, Y.-H.; Diau, E. W.-G., Energy Environ. Sci. 2018.
(37). Ran, C.; Xi, J.; Gao, W.; Yuan, F.; Lei, T.; Jiao, B.; Hou, X.; Wu, Z., ACS Energy Lett. 2018, 3, 713-721.
(38). Kim, H.; Lee, Y. H.; Lyu, T.; Yoo, J. H.; Park, T.; Oh, J. H., J. Mater. Chem. A 2018.
(39). Gupta, S.; Cahen, D.; Hodes, G., J. Phys. Chem. C 2018, 122, 13926-13936.
(40). Brown, N. D.; Chirafisi, A.; Levey, P. R. Limiting the loss of tin through oxidation in tin or tin alloy electroplating bath solutions. US Patent, No.6923899B2, 2005.
(41). Liu, Z.; Cao, M.; Chen, Y.; Fan, Y.; Wang, D.; Xu, H.; Wang, Y., J. Phys. Chem. B 2016, 120, 4102-4113.
(42). Wang, Q.; Zheng, X.; Deng, Y.; Zhao, J.; Chen, Z.; Huang, J., Joule 2017, 1, 371-382.
(43). Lee, J.-W.; Kim, H.-S.; Park, N.-G., Acc. Chem. Res. 2016, 49, 311-319.
(44). Chen, Z. Y.; Chan, P. T.; Ho, K. Y.; Fung, K. P.; Wang, J., Chem. Phys. Lipids 1996, 79, 157-163.
(45). Sroka, Z.; Cisowski, W., Food Chem. Toxicol. 2003, 41, 753-758.
(46). Shishlov, N. M.; Khursan, S. L., J. Mol. Struct. 2016, 1123, 360-366.
(47). Kato, Y.; Ono, L. K.; Lee, M. V.; Wang, S.; Raga, S. R.; Qi, Y. Adv. Mater. Inter. 2015, 2, 1500195.
(48). Zhang, H.; Chen, J. Q.; Lin, F.; He, H. X.; Mao, J.; Wong, K. S.; Jen, A. K-Y.; Choy, W. C. H. ACS Nano 2016, 10, 1503-1511.